Research Square

Preprints are preliminary reports that have not undergone peer review.
They should not be considered conclusive, used to inform clinical practice,
or referenced by the media as validated information.

Solar filament migration across activity cycles: The emergence of a late-cycle high-latitude population

Jouni Takalo

jojuta@gmail.com

Research Article

Keywords: Sun: filaments, Sun: activity, Sun: magnetic field, Sun: sunspots, Sun: evolution

Posted Date: September 15th, 2026

DOI: https://doi.org/10.21203/rs.3.rs-10881177/v1

License: This work is licensed under a Creative Commons Attribution 4.0 International License.
Read Full License

Additional Declarations: No competing interests reported.

Solar filament migration across activity cycles: The emergence of a late-cycle high-latitude population

Jouni J. Takalo

© The author(s) ●●●●

Abstract We investigate the latitude–time evolution of solar filament area over Solar Cycles 15–24 using the composite Hα filament record covering 1909–2022. Phase-normalized cycle distributions show the expected equatorward migration of the dominant low- and intermediate-latitude filament population together with a distinct high-latitude component emerging late in the cycle. The resulting late-cycle rise in mean filament latitude reflects the increasing contribution of this high-latitude population rather than a reversal of the main equatorward migration.
We compare its onset with independently identified sunspot butterfly wings of the following cycles. The first following-cycle sunspot groups occur later in eight of nine cycle transitions, by an average of approximately 1.1 yr. Persistent following-cycle sunspot-wing activity occurs later in all nine transitions, by approximately 2.2 yr, and this ordering is robust to changes in the persistence criterion. The results suggest that the late-cycle high-latitude filament population traces the transition between successive activity cycles.

Keywords: Sun: filaments; Sun: activity; Sun: magnetic field; Sun: sunspots; Sun: evolution

1. Introduction

Solar filaments are cool and dense plasma structures suspended in the solar corona by magnetic fields. When observed against the solar disk, they appear as dark elongated structures, whereas the same structures seen above the limb are referred to as prominences. Filaments are closely associated with polarity-inversion lines of the photospheric magnetic field and therefore provide useful tracers of the large-scale magnetic structure of the Sun (Tandberg-Hanssen 1995; Mackay et al. 2010; Labrosse et al. 2010; Gibson 2018). Unlike sunspots, which are concentrated mainly at low and intermediate latitudes, filaments occur over a much wider

Taivalkuja 12 b, FI-90910 Kontio
(e-mail: jojuta@gmail.com)

range of heliographic latitudes and can consequently provide information on the evolution of both active-region and large-scale background magnetic fields.

The latitude distribution of solar activity changes systematically during the solar cycle. The familiar sunspot butterfly diagram is dominated by activity bands that emerge at intermediate latitudes and migrate progressively toward the equator. Filaments show a more complex latitude–time pattern. Historical prominence and filament observations already revealed both equatorward- and poleward-moving branches (Bocchino 1933). Subsequent studies have confirmed that low- and intermediate-latitude filaments generally migrate toward the equator, while high-latitude filaments form a distinct poleward-moving branch (Minarovjech et al. 1998; Li et al. 2008; Li 2010).

The high-latitude branch is particularly important for the evolution of the global solar magnetic field. Polar-crown filaments form along polarity-inversion lines separating the polar magnetic flux from lower-latitude flux systems. Their poleward migration, commonly referred to as the "rush to the poles", is closely related to the evolution and reversal of the polar magnetic fields (Hyder 1965; Shimojo et al. 2006; Petrie 2015). Long-term prominence observations have shown that the poleward branch can be followed over many solar cycles and that its migration rate changes as the structures approach the poles (Chatterjee et al. 2020). Filament distributions therefore provide a complementary view of the solar cycle to that obtained from sunspots alone.

The coexistence of equatorward and poleward branches also emphasizes that the solar magnetic cycle cannot always be represented as a sequence of isolated 11-year activity intervals. Evidence for overlapping activity cycles has been found in several tracers of solar magnetism, including filaments and prominences. In particular, historical filament observations show that signatures associated with successive cycles may coexist in different latitude bands (Bocchino 1933; Mouradian and Soru-Escaut 1994). This behaviour forms part of the broader phenomenology usually referred to as the extended solar cycle, in which magnetic activity associated with consecutive cycles overlaps substantially in time and latitude (Li et al. 2008; McIntosh et al. 2021). Sunspot butterfly wings themselves also overlap across conventional cycle boundaries, since the first sunspot groups of a new cycle may appear at higher latitudes before the preceding low-latitude activity has disappeared. A comparison between the timing of high-latitude filament activity and the emergence of the following sunspot butterfly wing may therefore help to clarify whether the late-cycle filament population is related to the transition between successive activity cycles.

Several statistical studies have quantified the latitudinal evolution of filaments over individual or multiple solar cycles. Using the Meudon Cartes Synoptiques for Solar Cycles 16–21, Li (2010) showed that the low-latitude filament population migrates systematically toward the equator, but that its latitude evolution differs from that of sunspot groups. Filaments occur at higher latitudes than sunspots during a substantial part of the cycle, and their latitudinal drift does not follow the same simple evolution as the sunspot belts. Earlier analyses likewise identified separate equatorward and poleward prominence branches (Minarovjech et al. 1998), while radio observations demonstrated the close relationship between

high-latitude prominence activity and the evolution of the polar magnetic field (Shimojo et al. 2006; Shimojo 2013).

More recently, long historical observing series have made it possible to examine these patterns over many consecutive cycles. Chatterjee et al. (2020) studied the time–latitude distribution of prominences over Solar Cycles 15–24 using observations from Kodaikanal, Meudon, and Kanzelhöhe, and found systematic poleward migration over all ten cycles. The long-term Hα archive has also recently been analysed by Chatzistergos et al. (2023b), who constructed a composite filament-area record from multiple observatories covering 1909–2022. Their filament-area butterfly diagram clearly displays both the poleward migration of high-latitude structures and the progressive decrease of the mean filament latitude during the solar cycle.

These long-term observations raise an interesting question concerning the apparent late-cycle evolution of the filament latitude distribution. A mean latitude calculated from the complete filament population can be affected simultaneously by the equatorward migration of the established low-latitude population and by the appearance of high-latitude structures associated with the evolving large-scale magnetic field. Consequently, an increase in mean filament latitude near the end of a conventionally defined solar cycle does not necessarily imply a reversal of the equatorward migration. It may instead reflect the increasing contribution of a high-latitude population while low-latitude structures from the ongoing cycle are still present.

The availability of a homogeneous long-term filament-area record provides an opportunity to examine this behaviour statistically over many solar cycles. Rather than treating each cycle only in calendar time, the cycles can be transformed to a common normalized phase coordinate. Such a representation allows recurrent latitude structures to be separated from differences in individual cycle duration and makes it possible to determine whether features seen near cycle boundaries are systematic or dominated by a small number of cycles.

In this work, we investigate the latitude distribution and migration of solar filament area over Solar Cycles 15–24. We first examine the long-term latitude–time distribution and then transform the individual cycles to a common normalized phase. We use the phase-normalized distributions to determine the mean filament migration pattern and its cycle-to-cycle stability. Particular attention is given to the late-cycle increase in mean absolute latitude. By separating low- and high-latitude filament area, we test whether this increase represents a poleward reversal of the main filament population or the growing contribution of high-latitude filaments. Finally, we examine the phase dependence of filament area in different latitude bands and in the two solar hemispheres.

2. Data and methods

2.1. Filament data

We use the long-term composite Hα filament-area data set constructed by Chatzistergos et al. (2023b) and distributed through CDS/VizieR (Chatzistergos

et al. 2023a). The data set covers 1909–2022 and was constructed from full-disc Hα observations from 15 historical and modern archives. The individual archives were processed consistently, and the filament areas were cross-calibrated by scaling them to the Meudon series before constructing the composite.

The CDS/VizieR file `comp.dat` contains daily values of projected filament area in 180 heliographic latitude bins of 1° width, extending from −90° to +90°. For each observing day, the file gives the calendar date and decimal year followed by the filament areas in the 180 latitude bins. According to the catalogue documentation, the areas represent fractions of the projected solar-disc area.

The numerical filament-area values in the distributed data file require an additional factor of 10^{-3} to obtain the corresponding fraction of the projected solar-disc area (T. Chatzistergos, private communication). We apply this factor when filament areas are expressed in physical fractional-area units. The factor has no effect on the normalized latitude distributions, area-weighted mean latitudes, fractional contributions of different latitude bands, or the onset times derived below, because it is a common multiplicative factor for all filament-area values.

The present analysis covers Solar Cycles 15–24. The conventional cycle boundaries were taken to be August 1913, August 1923, September 1933, February 1944, April 1954, October 1964, March 1976, September 1986, August 1996, December 2008, and December 2019. Thus, SC15–SC23 are analysed from one conventional sunspot minimum to the next, while SC24 is included up to the December 2019 minimum. Although the filament composite extends through 2022, observations after the December 2019 minimum are not assigned to SC24 in the cycle-normalized analysis.

No attempt was made to identify or track individual filament structures. Instead, the analysis is based on the total projected filament area in each latitude bin. The resulting distributions therefore describe the statistical latitude–time evolution of filament area rather than trajectories of individual filaments.

2.2. Solar-cycle phase normalization

Because solar-cycle durations vary appreciably, direct averaging in calendar time would blur recurrent structures occurring at different relative times within individual cycles. We therefore transformed each cycle to a common normalized phase coordinate. For an observation at time t within cycle i, the normalized phase was defined as

$$\phi = \frac{t - t_{\mathrm{start},i}}{t_{\mathrm{end},i} - t_{\mathrm{start},i}}, \tag{1}$$

where $t_{\mathrm{start},i}$ and $t_{\mathrm{end},i}$ denote the conventional sunspot minima bounding the cycle. Thus, $\phi = 0$ corresponds to the beginning of a cycle and $\phi = 1$ to the following minimum.

For the phase-normalized distributions, the interval $0 \leq \phi < 1$ was divided into 40 equal bins, corresponding to a phase resolution of 0.025. The same phase grid was used for all cycles. This procedure allows filament distributions from cycles of different duration to be compared directly and averaged without imposing a common duration in physical time.

2.3. Latitude distributions and filament-area weighting

The filament butterfly distributions were constructed from the observed filament area in each latitude bin. For a given phase bin, the filament areas of all observations falling within that interval were accumulated separately at each heliographic latitude. The resulting latitude–phase distribution therefore represents filament area rather than the number of individual filament detections.

To characterize the typical latitude of the filament population, we calculated the area-weighted mean absolute latitude,

$$\langle|\lambda|\rangle = \frac{\sum_j A_j|\lambda_j|}{\sum_j A_j}, \tag{2}$$

where A_j is the filament area in latitude bin j and λ_j is the corresponding heliographic latitude. The use of absolute latitude allows the overall migration pattern to be examined without cancellation between the northern and southern hemispheres. Northern and southern hemispheres were also analysed separately where required.

To distinguish the contributions of different parts of the latitude distribution, the filament area was also integrated over selected latitude ranges. In particular, low-latitude and high-latitude components were examined separately. The high-latitude population used in the onset analysis was defined by $|\lambda| \geq 50°$. This threshold is intended as an operational definition of high-latitude filament activity and does not imply that all structures included in this population are polar-crown filaments.

2.4. Cycle-to-cycle variability

The recurrence of the phase-dependent filament pattern was assessed by calculating the latitude distributions separately for each solar cycle. Each cycle distribution was normalized independently before the cycle ensemble was averaged. This prevents cycles with larger total filament area from dominating the mean distribution and allows the persistence of latitude–phase structures to be evaluated across the cycle sample.

Cycle-to-cycle variability was further examined from the area-weighted mean latitude and from the fractional filament area in different latitude bands. The latter was calculated as the area in a given latitude interval divided by the total filament area in the corresponding phase bin. Northern and southern hemispheres were treated separately when testing the timing of the high-latitude population.

2.5. Onset of late-cycle high-latitude filament activity

To quantify the appearance of the late-cycle high-latitude filament population, we calculated, separately for each hemisphere, the fraction of filament area located at $|\lambda| \geq 50°$ in each phase bin. The onset search was restricted to the late part of the cycle, $\phi \geq 0.65$.

For each cycle and hemisphere, a relative onset threshold was defined from the minimum and maximum high-latitude filament fractions within the late-cycle interval. The filament-activity threshold, $f_{\rm th}$, was defined as

$$f_{\rm th} = f_{\rm min} + 0.20\,(f_{\rm max} - f_{\rm min})\,. \tag{3}$$

Here, $f_{\rm min}$ and $f_{\rm max}$ denote the minimum and maximum values of the filament activity measure f, respectively. Thus, $f_{\rm th}$ corresponds to a level 20% above the minimum within the observed range from $f_{\rm min}$ to $f_{\rm max}$. The threshold is therefore defined relative to the dynamic range of the filament activity rather than as 20% of its absolute maximum value. The 20% level was chosen to identify the initial sustained increase in filament activity while avoiding fluctuations close to the background minimum.

The filament onset was defined as the first of two consecutive phase bins for which the high-latitude fraction exceeded this threshold. Requiring two consecutive bins reduces the sensitivity of the onset time to isolated short-lived enhancements. The use of a relative rather than an absolute threshold also reduces sensitivity to differences in filament activity level between individual cycles.

The sensitivity of the filament onset to the precise definition of high-latitude activity was examined by varying the latitude threshold and relative onset level. The qualitative temporal behaviour was found to persist under these changes, and $|\lambda| \geq 50^\circ$ and a relative level of 0.20 were adopted for the reference analysis.

2.6. Sunspot butterfly-wing data

To compare the late-cycle filament population with the development of the following sunspot cycle, we used the separated sunspot butterfly wings of Leussu et al. (2017b) and the associated CDS/VizieR data set (Leussu et al. 2017a). The catalogue contains sunspot-group observations from 1826–2015 and assigns the groups to individual northern and southern butterfly wings for Solar Cycles 7–24.

The separation of overlapping sunspot butterfly wings is based on the method developed by Leussu et al. (2016). The method uses long gaps in sunspot-group occurrence in different latitude bands to define the boundaries between successive hemispheric wings. This allows individual sunspot groups to be assigned to a specific solar-cycle wing and, in particular, permits the overlapping old- and new-cycle populations near sunspot minimum to be separated. We use the published wing assignments directly and do not attempt to distinguish old- and new-cycle sunspot groups using a latitude threshold of our own.

The extended wing catalogue of Leussu et al. (2017b) combines historical sunspot observations by Schwabe and Spörer with the Royal Greenwich Observatory and SOON records. For the interval relevant to the present analysis, the sunspot groups are therefore already assigned to individual northern or southern solar-cycle wings in the published catalogue.

The filament–sunspot comparison was performed for SC15–SC23. For each of these filament cycles, the high-latitude filament onset was compared with the onset of the sunspot butterfly wing of the following cycle, i.e. SC15 filaments were compared with the SC16 sunspot wing, and so forth through SC23 filaments

and the SC24 sunspot wing. SC24 cannot be used as a preceding filament cycle in this comparison because the wing catalogue does not contain the following SC25 wing.

Sunspot-wing times were expressed in the normalized phase of the preceding filament cycle. Values exceeding $\phi = 1$ are therefore possible and indicate that the corresponding following-cycle sunspot activity became established after the conventional minimum separating the two cycles.

2.7. Sunspot-wing onset definitions

Two measures were used to characterize the beginning of a following sunspot butterfly wing. The first-wing onset was simply the earliest sunspot-group observation assigned by the catalogue to the following wing in the corresponding hemisphere. This measure captures the earliest identified following-cycle activity, but its timing may be determined by a single isolated group appearing before the following wing becomes persistently established.

We therefore also defined a more conservative persistent-wing onset. For the reference analysis, sunspot-group observations were binned in 3-month intervals, and persistent activity was defined as occurrence in two consecutive occupied bins. The onset was assigned to the first bin of the first such sequence. The first-group and persistent-wing definitions consequently characterize two different stages of the development of the following sunspot cycle: its earliest identified sunspot occurrence and the establishment of sustained wing activity, respectively.

2.8. Statistical tests and robustness

For each cycle and hemisphere, the temporal difference was calculated as

$$\Delta\phi = \phi_{\mathrm{spot}} - \phi_{\mathrm{filament}}, \tag{4}$$

so that $\Delta\phi > 0$ indicates that the high-latitude filament onset preceded the onset of the following sunspot wing.

Because the northern and southern hemispheres of a given solar cycle cannot be assumed to represent fully independent realizations, the primary statistical tests were performed at the solar-cycle level. The northern and southern onset differences were averaged within each cycle, giving nine cycle-level values for SC15–SC23.

The significance of the mean temporal ordering was evaluated using an exact sign-flip randomization test. With nine cycles, all $2^9 = 512$ possible sign combinations can be evaluated explicitly, avoiding any assumption of a normal sampling distribution. Two-sided probabilities are reported. Uncertainty in the mean and median phase differences was also evaluated using a non-parametric cycle bootstrap, in which entire solar cycles, with their northern and southern measurements kept together, were resampled with replacement. A total of 50 000 bootstrap realizations were used, and percentile-based 95% confidence intervals were calculated.

The influence of individual cycles was tested with a leave-one-cycle-out analysis. In addition, the robustness of the persistent-wing onset was tested by varying

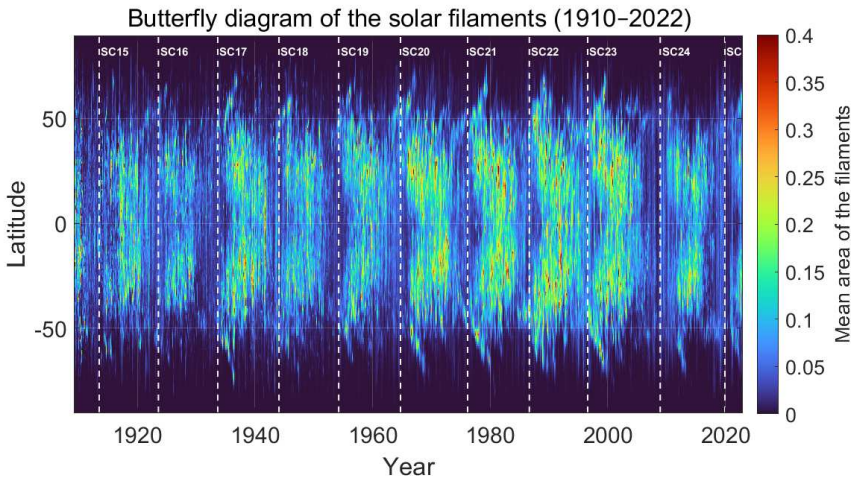


Figure 1. Latitude–time distribution of solar filament area in the COMP data for 1910–2022. The vertical dashed lines indicate the adopted boundaries of Solar Cycles 15–24.

the sunspot time-bin width between 2, 3, and 4 months and requiring activity in either two or three consecutive bins. This gives six alternative definitions of persistent wing activity. The resulting range of onset differences is used to assess the sensitivity of the inferred filament lead to the precise persistence criterion.

For physical interpretation, normalized phase differences were also converted to approximate time differences using the actual duration of each preceding solar cycle. These time differences are used only to express the magnitude of the observed lead in years; the statistical tests themselves were performed using normalized cycle phase.

3. Results

3.1. Long-term latitude–time distribution of filament area

Figure 1 shows the latitude–time distribution of filament area in the COMP data over 1910–2022. The filament distribution exhibits the well-known butterfly-like pattern, with activity concentrated predominantly at low and intermediate heliographic latitudes and additional branches extending to higher latitudes.

The low- and mid-latitude filament populations show a systematic migration toward the equator during the solar cycle. At the same time, high-latitude filament activity is particularly evident near the transition between consecutive cycles. The latitude–time diagram therefore indicates substantial temporal overlap between filament populations belonging to successive phases of solar activity.

The vertical dashed lines in Fig. 1 indicate the adopted solar-cycle boundaries. These boundaries are used below to transform each cycle to a common normalized phase coordinate and to compare the latitude evolution of Solar Cycles 15–24.

3.2. Phase-normalized filament butterfly

To compare filament migration between solar cycles of different durations, each cycle was mapped onto a normalized phase interval $0 \leq \phi \leq 1$, where $\phi = 0$ and $\phi = 1$ correspond to consecutive solar-cycle boundaries. The filament-area distributions were then averaged over Solar Cycles 15–24.

Figure 2(a) shows the resulting mean phase-normalized butterfly diagram. The averaging preserves a pronounced and highly organized latitude evolution. At the beginning of the normalized cycle, filament area is distributed over a broad latitude range. A prominent concentration occurs at approximately $|\lambda| \sim 20°$–$35°$, followed by a gradual migration toward lower latitudes as the cycle progresses.

The phase-normalized diagram also reveals substantial high-latitude filament area during the early part of the cycle. The high-latitude filament fraction reaches a minimum during the declining phase and subsequently increases again toward the end of the cycle. In the phase-normalized butterfly diagram, this increase is associated with filament activity at latitudes clearly separated from the low-latitude branch approaching the cycle minimum. This suggests the emergence of a distinct high-latitude filament population late in the cycle.

To quantify this behaviour, the northern and southern hemispheres were folded into absolute latitude, $|\lambda|$. Figure 2(b) shows the mean filament-area distribution in the $(\phi, |\lambda|)$ plane. The white curve with a black dashed outline gives the area-weighted mean absolute latitude, $\langle|\lambda|\rangle$, as defined in Eq. (2).

The mean latitude initially increases, reaching approximately 32° during the early phase of the cycle. It subsequently decreases to about 23° during the declining phase. However, this decrease does not continue until the end of the cycle. Instead, the mean absolute latitude turns upward again during the late part of the cycle and reaches approximately 29° close to the following cycle boundary.

3.3. Cycle-to-cycle stability of the latitude distribution

The similarity of the filament latitude distributions between individual cycles was examined by integrating the filament area over each complete solar cycle. For this comparison, the latitude distribution of each cycle was normalized by its total filament area,

$$f_c(\lambda) = \frac{A_c(\lambda)}{\sum_\lambda A_c(\lambda)}, \tag{5}$$

so that

$$\sum_\lambda f_c(\lambda) = 1. \tag{6}$$

Consequently, Fig. 3 compares the shapes of the latitude distributions rather than the absolute filament activity of different cycles.

Despite considerable differences in solar-cycle amplitude and duration, the latitude distributions of SC15–SC24 have remarkably similar overall shapes.

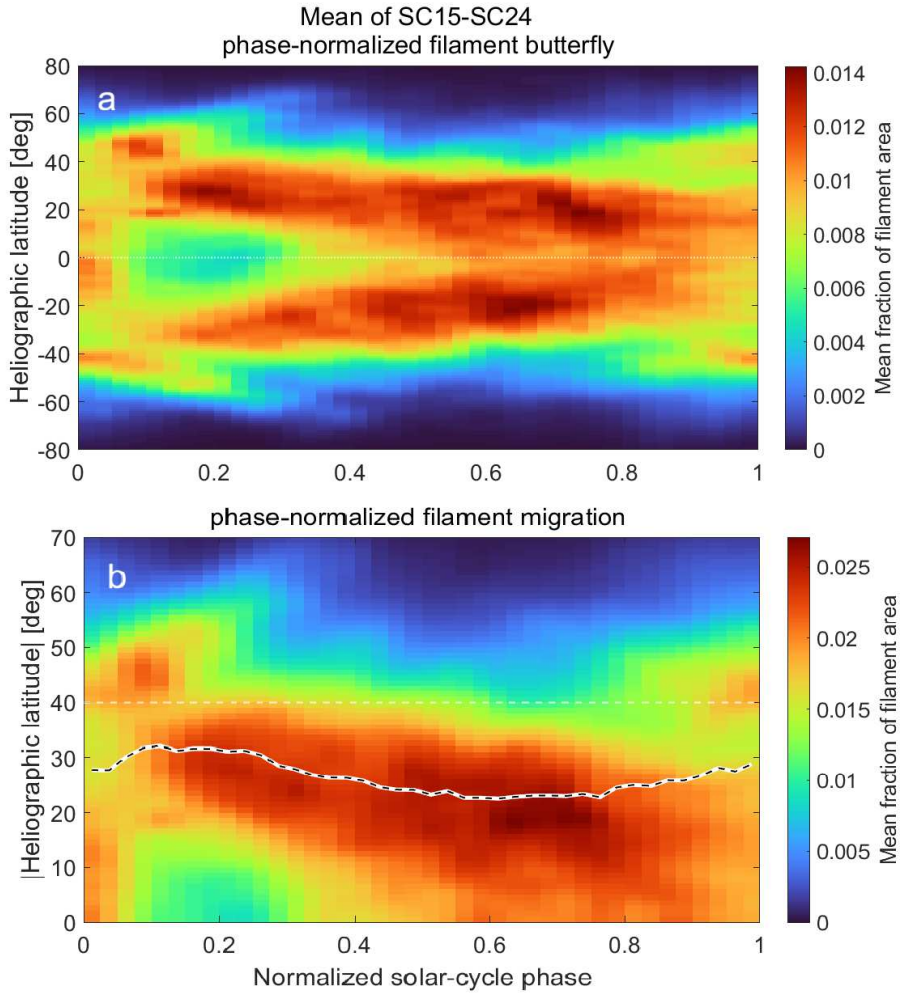


Figure 2. Phase-normalized filament migration averaged over Solar Cycles 15–24. (a) Mean latitude–phase distribution retaining the northern and southern hemispheres separately. (b) Corresponding distribution after folding the hemispheres into absolute latitude. The solid curve gives the area-weighted mean $|\lambda|$. The horizontal dashed line marks $|\lambda| = 40°$.

All cycles show two broad maxima in the northern and southern hemispheres, typically located near $|\lambda| \sim 20°$–$30°$, together with a relative minimum near the equator. The distributions also possess extended high-latitude tails.

The thick curve in Fig. 3 represents the mean of the ten individually normalized cycle distributions. The close clustering of the individual curves around this mean indicates that the basic latitude structure of the filament population is a persistent feature across the analysed solar cycles.

Some cycle-to-cycle differences are nevertheless present, particularly in the relative strengths and precise latitudes of the northern and southern maxima.

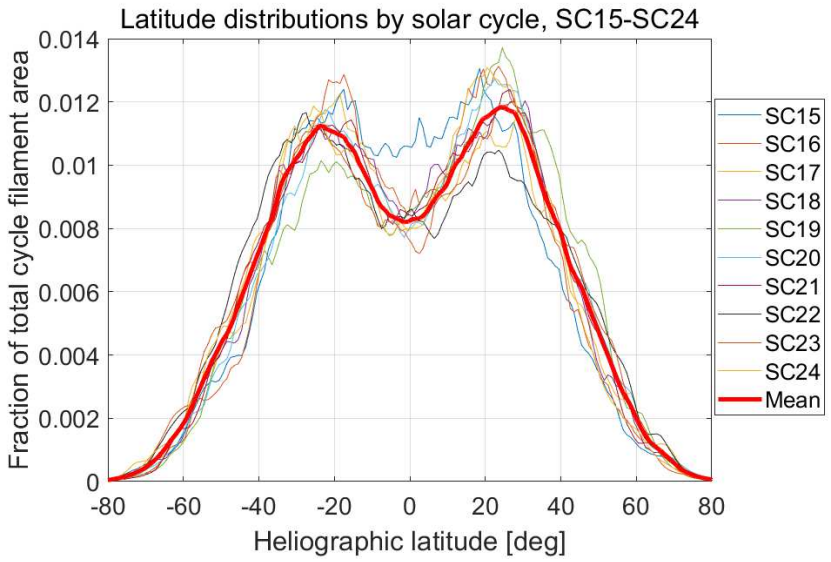


Figure 3. Normalized filament-area distributions as a function of heliographic latitude for Solar Cycles 15–24. Each cycle has been normalized independently to unit total area. The thick curve shows the mean of the ten cycle distributions.

These variations are considerably smaller than the common large-scale structure shared by the cycles.

3.4. Origin of the late-cycle increase in mean latitude

The late-cycle increase in the area-weighted mean latitude seen in Fig. 2(b) could, in principle, result either from a reversal of the equatorward migration of the main filament population or from an increasing contribution of a separate high-latitude population. These possibilities can be distinguished by separating the filament area at $|\lambda| = 40°$.

Figure 4(a) shows the area-weighted mean latitude when only filament area at $|\lambda| < 40°$ is included. The restricted population shows the expected decrease from approximately 23° during the early cycle to about 18°–19° during the declining phase. Most importantly, the strong late-cycle increase seen when all latitudes are included is largely absent. The low-latitude population therefore does not undergo a substantial poleward reversal.

Figure 4(b) provides the complementary test. It shows the fraction of the total filament area located at $|\lambda| \geq 40°$. The high-latitude fraction is large during the early part of the normalized cycle, decreases systematically during the subsequent evolution, and reaches a broad minimum around $\phi \sim 0.55$–0.65. It then increases again toward the end of the cycle, with the increase becoming especially pronounced during the late declining phase.

The individual-cycle curves demonstrate that this behaviour is not produced by a single anomalous solar cycle. A late-cycle increase of the high-latitude filament-area fraction is found in all Solar Cycles 15–24.

These results demonstrate that the late-cycle increase in the mean absolute filament latitude is primarily caused by the increasing contribution of high-latitude filaments rather than by a reversal of the equatorward migration of the low-latitude filament population. In the full butterfly diagram, these high-latitude structures appear while low-latitude filament activity from the ongoing cycle is still present. This behaviour demonstrates an overlap between the declining low-latitude filament population and an emerging high-latitude population. The possible relation of the latter to the following sunspot cycle is examined in Sect. 3.6.

3.5. Filament area in different latitude bands

To examine the phase dependence of the filament distribution in more detail, we divided the filament area into three latitude ranges, 0°–30°, 30°–55°, and 55°–75°, separately for the northern and southern hemispheres. Figure 5 shows the mean projected filament area as a function of normalized solar-cycle phase for SC15–SC24.

The three latitude ranges exhibit clearly different temporal evolution. The high-latitude component (55°–75°) is strongest during the early phase of the cycle and decreases rapidly thereafter, reaching very low levels during the middle part of the cycle. A modest increase is visible again toward the end of the cycle. The intermediate-latitude component (30°–55°) reaches its largest values earlier than the low-latitude component and subsequently declines. In contrast, the 0°–30° component continues to increase toward the activity maximum and remains the dominant contribution during a large part of the cycle. The same general evolution is observed in both hemispheres.

A weak temporary depression of the low-latitude filament area is also visible near the maximum phase of the cycle, around $\phi \simeq 0.38$ (Fig. 5). Its timing is close to the mean phase of the Gnevyshev gap (GG) found previously in sunspot-group areas and related solar and geomagnetic activity indices (Takalo 2021a,b). The filament data show qualitatively similar behaviour, but the phase of the depression varies considerably among individual cycles. We therefore do not attempt an independent identification or characterization of the Gnevyshev gap from the filament data.

3.6. Relation to the onset of the following sunspot cycle

The late-cycle increase of high-latitude filament activity raises the question of whether this population is related to the development of the following solar cycle. To examine this possibility, we compared the onset of high-latitude filament activity with the independently determined butterfly wings of sunspot groups. The comparison was restricted to SC15–SC23 because identification of a following-cycle sunspot wing is required; the sunspot-wing catalogue extends through SC24.

For each hemisphere and solar cycle, the onset of the high-latitude filament population was determined from the filament-area distribution. The timing was expressed in the normalized phase of the preceding sunspot cycle. The

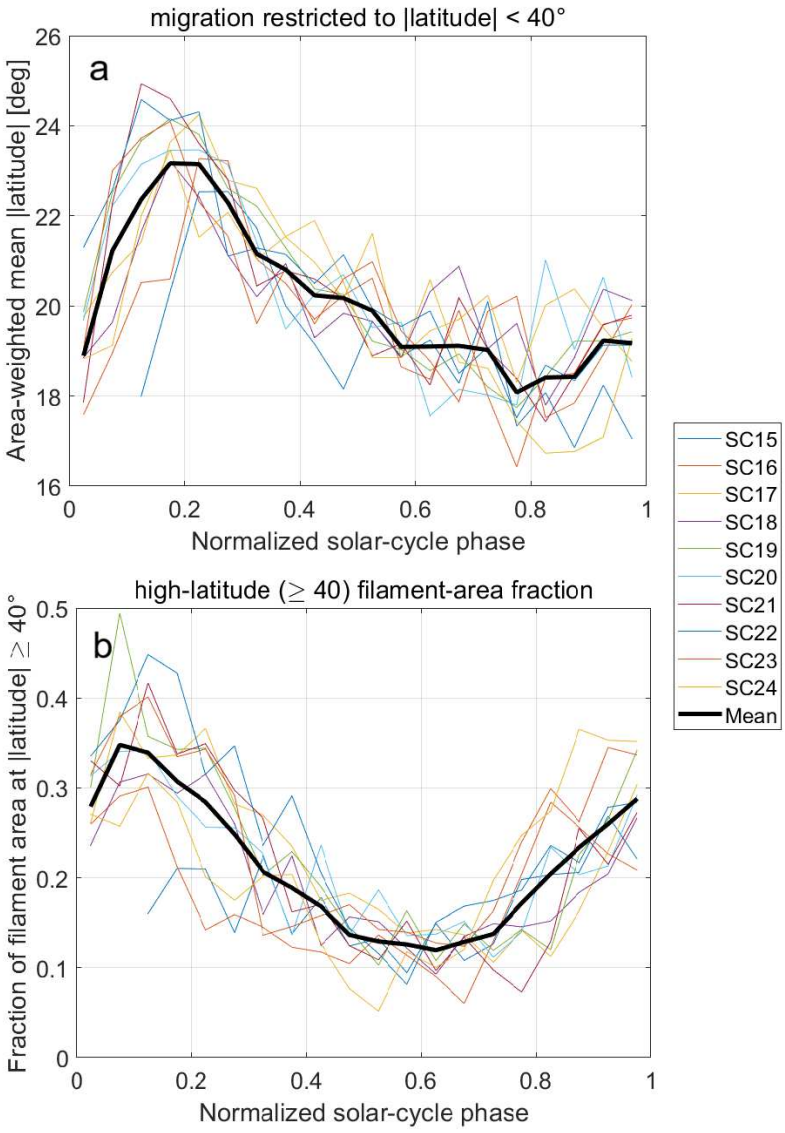


Figure 4. Separation of the low- and high-latitude filament populations. (a) Area-weighted mean absolute latitude calculated using only filament area at $|\lambda| < 40°$. Thin curves show individual Solar Cycles 15–24 and the thick curve their mean. (b) Fraction of the total filament area located at $|\lambda| \geq 40°$. The high-latitude contribution reaches a minimum during the middle-to-late part of the cycle and increases again toward the subsequent cycle boundary.

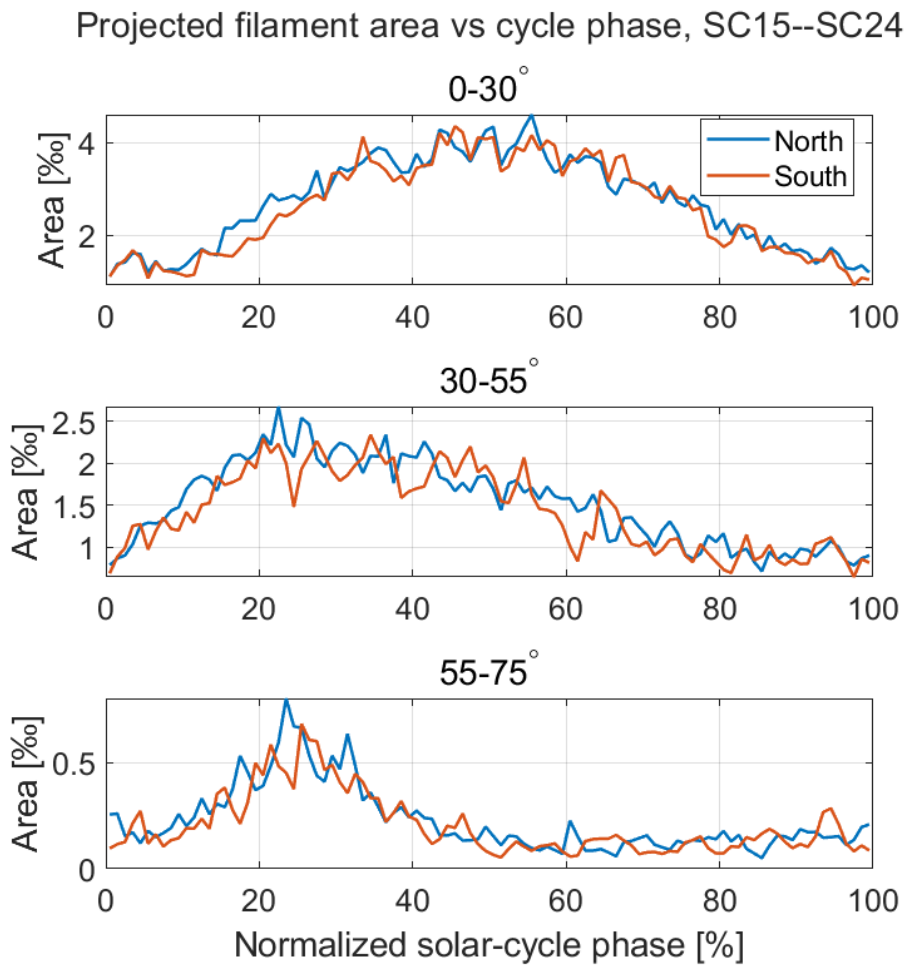


Figure 5. Mean projected filament area as a function of normalized solar-cycle phase for three latitude ranges, shown separately for the northern and southern hemispheres. Note that the vertical scales differ between the panels to emphasize the phase dependence at higher latitudes.

corresponding onset of the following-cycle sunspot wing was determined in two ways. First, we used the first sunspot group assigned to the following butterfly wing. Second, a more conservative persistent-wing onset was defined as the first of two consecutive 3-month bins containing sunspot-group observations assigned to the following-cycle wing. Thus, the first-group criterion identifies the earliest observational signature of the following sunspot cycle, whereas the persistent criterion marks the establishment of sustained sunspot activity.

Figure 6 compares the filament onset with the first following-cycle sunspot groups for SC15–SC23. In most cycles and in both hemispheres, the high-latitude filament population appears before the first sunspot groups belonging to the following butterfly wing. Averaging the two hemispheres within each cycle, the first-wing onset occurs after the filament onset in eight of the nine cycles. The

Table 1. Robustness of the temporal ordering between high-latitude filament onset and persistent following-cycle sunspot-wing onset. The persistence criterion was varied by changing the temporal bin size and the number of consecutive occupied bins required. Positive phase differences indicate that the sunspot-wing onset occurs after the filament onset.

Bin size (months)	Consecutive bins required	Mean phase difference (spot–filament)	Mean lead time (yr)
2	2	0.205	2.15
2	3	0.227	2.40
3	2	0.193	2.03
3	3	0.201	2.12
4	2	0.178	1.88
4	3	0.188	1.99

mean difference is 0.105 in normalized cycle phase, corresponding to approximately 1.1 yr. An exact cycle-level sign-flip randomization test gives $p = 0.0078$ (two-sided), and the bootstrap 95% confidence interval for the mean difference is 0.060–0.145.

The temporal ordering becomes still more systematic when the onset of persistent sunspot-wing activity is considered. The persistent wing appears after the high-latitude filament onset in all nine cycles SC15–SC23. The mean phase difference is 0.206, corresponding to approximately 2.2 yr. An exact cycle-level sign-flip randomization test gives $p = 0.0039$ (two-sided). A cycle bootstrap gives a 95% confidence interval of 0.183–0.235 for the mean phase difference.

The result is not controlled by any individual solar cycle. In a leave-one-cycle-out analysis, the mean first-wing delay remains between 0.092 and 0.122 in normalized phase, while the persistent-wing delay remains between 0.193 and 0.211.

We also tested the sensitivity of the persistent-wing result to its definition. Temporal bin widths of 2, 3, and 4 months were combined with requirements of activity in either two or three consecutive bins. For all six definitions, the persistent sunspot-wing onset followed the filament onset in all nine cycle transitions. The mean phase difference ranged from 0.178 to 0.227, corresponding to a mean filament lead time of 1.88–2.40 yr (Table 1). The exact two-sided sign-flip probability was $p = 0.0039$ for all six definitions. Thus, both the temporal ordering and the magnitude of the filament lead are insensitive to reasonable changes in the definition of persistent sunspot-wing onset.

These results establish a systematic temporal sequence in which the late-cycle high-latitude filament population appears first, followed by the earliest sunspot groups of the next butterfly wing and, subsequently, by persistent following-cycle sunspot activity. The timing alone does not demonstrate that the high-latitude filaments belong magnetically to the following cycle. Nevertheless, the present results show that the appearance of the high-latitude filament population systematically precedes the development of the following sunspot butterfly wing.

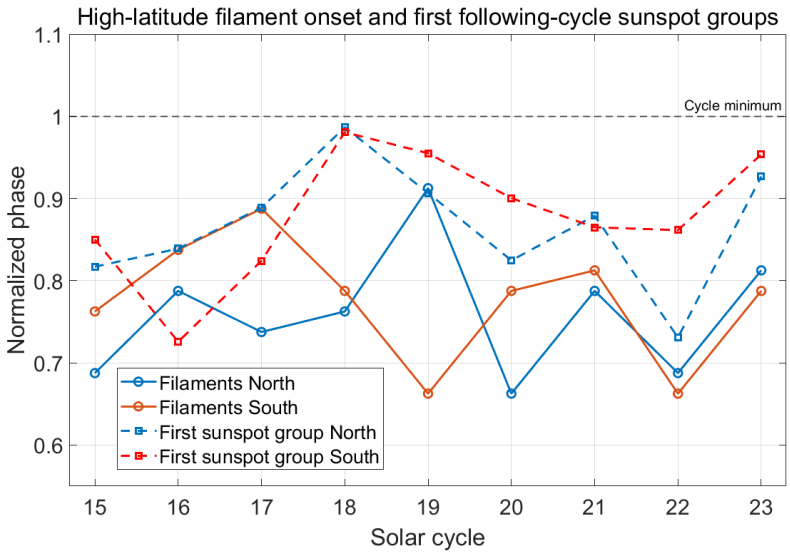


Figure 6. Onset of high-latitude filament activity and the first sunspot groups belonging to the following solar-cycle butterfly wing for SC15–SC23, shown separately for the northern and southern hemispheres. All times are expressed in the normalized phase of the preceding solar cycle. The horizontal dashed line at $\phi = 1$ marks the conventional cycle minimum. In most cycles, high-latitude filament activity appears before the first sunspot groups assigned to the following butterfly wing.

3.7. Summary of the observational results

The data reveal a coherent pattern of filament migration that is reproduced over Solar Cycles 15–24. The principal observational results can be summarized as follows.

First, the filament population exhibits a persistent butterfly-like latitude–time distribution, including both an equatorward-migrating low- and mid-latitude component and high-latitude filament activity. Second, after normalizing the individual cycles to a common phase, the mean filament latitude decreases through most of the cycle but increases again toward the following cycle boundary. Third, this late-cycle increase disappears to a large extent when filaments above 40° are excluded. At the same time, the fractional filament area above 40° increases strongly during the late part of the cycle. Finally, this high-latitude return is observed in each of the ten analysed cycles.

The phase-normalized results therefore reveal two overlapping components in the filament butterfly: a low-latitude population that predominantly migrates equatorward and a high-latitude population that becomes increasingly important before the end of the conventional solar-cycle interval.

Comparison with independently identified sunspot butterfly wings further shows that the late-cycle high-latitude filament population systematically precedes the development of the following sunspot cycle. The first following-cycle sunspot groups occur later in eight of nine cycles, while persistent following-cycle sunspot activity occurs later in all nine cycles. The latter follows the filament onset

by approximately two years, with the result remaining stable under different definitions of persistent sunspot-wing onset.

Together, these results demonstrate a systematic overlap between the declining low-latitude filament population and an emerging high-latitude population whose appearance precedes the following sunspot butterfly wing. The physical interpretation of this high-latitude population and its relation to the evolution of the solar magnetic cycle are considered in the following section.

4. Discussion

4.1. The late-cycle increase in filament latitude

The phase-normalized analysis reveals a systematic increase in the mean absolute filament latitude during the declining part of the solar cycle. At first sight, such an increase might be interpreted as a change in the direction of filament migration. The latitude-resolved distributions, however, show that this interpretation is not appropriate. The dominant low- and intermediate-latitude filament population continues its overall equatorward evolution, while a separate high-latitude population becomes increasingly visible late in the cycle. The increase in the mean latitude is therefore primarily a population-mixing effect rather than a poleward reversal of the main equatorward branch.

This distinction is important when filament migration is characterized by a single mean latitude. Filaments occupy a substantially broader latitude range than sunspots and include structures associated with different components of the large-scale magnetic field. A mean latitude consequently combines populations with different time–latitude evolution. In particular, the simultaneous presence of declining low-latitude activity and emerging high-latitude filament area can produce an increase in the mean latitude even though the low-latitude population itself continues to evolve equatorward.

Previous prominence and filament studies have identified both equatorward- and poleward-moving branches (Bocchino 1933; Minarovjech et al. 1998; Li et al. 2008; Li 2010), while the high-latitude poleward branch has been associated with the evolution of polar-crown prominences and the polar magnetic field (Shimojo et al. 2006; Shimojo 2013; Petrie 2015; Chatterjee et al. 2020). The present results are consistent with this general picture but emphasize a different aspect of the latitude distribution: the late-cycle high-latitude contribution can remain or re-emerge while the low-latitude filament population of the ongoing cycle is still present. Phase normalization makes this overlap particularly clear because recurrent structures from cycles of different duration are placed on a common temporal scale.

The operational high-latitude threshold used here, $|\lambda| \geq 50°$, should not be interpreted as identifying all of these structures as polar-crown filaments. Our result therefore concerns a statistical high-latitude filament population rather than a uniquely identified class of polar-crown filaments.

4.2. Relation to the transition between successive cycles

The comparison with the independently separated sunspot butterfly wings provides an additional constraint on the interpretation of the late-cycle high-latitude population. For SC15–SC23, the high-latitude filament onset generally occurs before the first sunspot groups assigned to the following butterfly wing. At the cycle level, the first following-cycle groups occur later in eight of nine cycles, with a mean separation of 0.105 in normalized phase, corresponding to approximately 1.1 yr.

The temporal ordering is even more systematic when the establishment of persistent following-cycle sunspot activity is considered. Persistent sunspot-wing activity follows the filament onset in all nine cycles, with a mean separation of about 0.21 in normalized cycle phase, or approximately 2.2 yr. The result is insensitive to the removal of individual cycles and remains essentially unchanged when the temporal binning and persistence criterion are varied. The observed ordering is therefore unlikely to be produced by a particular cycle or by the precise operational definition of persistent sunspot activity.

This comparison is useful because the sunspot-cycle assignment is not derived from the filament data. We use the independently separated butterfly wings of Leussu et al. (2017b), rather than assigning early high-latitude sunspots to cycles using our own latitude criterion. The filament–sunspot timing relation therefore reflects a comparison between two independently constructed descriptions of solar-cycle evolution.

The timing is, however, suggestive in the context of overlapping solar cycles. Successive activity cycles are known to overlap in time–latitude space, with signatures of a new cycle appearing before activity associated with the preceding cycle has disappeared (Bocchino 1933; Mouradian and Soru-Escaut 1994; Li et al. 2008; McIntosh et al. 2021). The present results extend this picture by showing that a high-latitude filament population can be detected systematically before the corresponding following-cycle sunspot wing becomes persistent. Filaments may therefore provide an observational tracer of changes in the large-scale magnetic configuration during the transition between successive cycles, before these changes are fully expressed by sustained sunspot emergence.

Solar filaments are closely associated with polarity inversion lines (PILs) separating regions of opposite magnetic polarity. Using MDI/SOHO magnetograms and a large sample of Hα filaments, Meunier and Delfosse (2011) found that the great majority of filaments are located close to PILs, confirming their close relationship with the large-scale magnetic-field configuration. A complementary long-term analysis of the McIntosh archive by Mazumder et al. (2018) showed that the spatial and temporal properties of filaments and their associated PILs vary systematically over the sunspot cycle, supporting the use of filament distributions as tracers of the evolving large-scale solar magnetic field. The magnetic nature of this association is further supported by spectropolarimetric observations showing systematic relationships between the magnetic-field orientation of filaments and the polarity configuration of the surrounding photospheric field (Hanaoka and Sakurai 2017). These results provide a physical basis for interpreting the high-latitude filament population identified here as a tracer of large-scale magnetic evolution, while not by themselves establishing its magnetic-cycle membership.

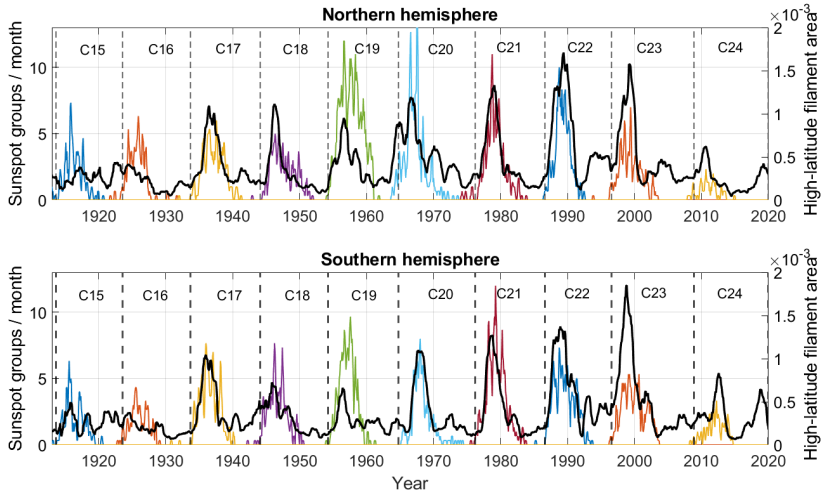


Figure 7. Calendar-time comparison of high-latitude filament activity and the high-latitude sunspot-group wings in the northern (top) and southern (bottom) hemispheres. Black curves show the 13-month smoothed monthly mean filament area at $|\lambda| \geq 50°$. Colored curves show the 3-month smoothed monthly occurrence of sunspot groups at $|\lambda| > 25°$, separated according to the solar-cycle assignments of Leussu et al. (2017b). Vertical dashed lines mark the conventional sunspot-cycle minima. The sunspot latitude threshold is used here only to emphasize the emergence of the high-latitude portion of each butterfly wing and is not used in the quantitative onset analysis.

Figure 7 illustrates this relationship directly in calendar time. The high-latitude filament area at $|\lambda| \geq 50°$ is compared with sunspot-group occurrence at $|\lambda| > 25°$, with the sunspot groups separated according to the independently assigned butterfly wings of Leussu et al. (2017b). The conventional sunspot-cycle minima are also shown. In several cycle transitions, enhanced high-latitude filament activity is already present before or near the conventional minimum and overlaps in time with the emergence of the high-latitude portion of the following sunspot butterfly wing. The 25° sunspot threshold is used here only to make the early high-latitude part of each butterfly wing visible and is not used in the quantitative onset analysis.

The calendar-time comparison reinforces the phase-normalized result: the late-cycle high-latitude filament population is not simply a poleward reversal of the main equatorward-migrating filament population. Instead, its occurrence during the interval in which the following sunspot wing begins to emerge is consistent with a large-scale magnetic reorganization during cycle overlap.

This connection provides a natural context for the results of Routh et al. (2025), who showed that polar filaments can trace interactions between large-scale magnetic flux systems associated with successive stages of the solar magnetic cycle. They interpreted polar filaments as forming where remnant magnetic flux from the preceding cycle interacts with poleward-transported flux of the ongoing cycle. They also found that polar-filament properties contain information related to the amplitude of the subsequent sunspot cycle.

The results of Routh et al. (2025) therefore provide a possible physical context for the temporal ordering found here. The systematic appearance of the high-latitude filament population before the first, and especially before the persistent, sunspot groups of the following butterfly wing suggests that the large-scale magnetic reorganization traced by high-latitude filaments is already underway before the following sunspot wing becomes established. This is consistent with an extended transition between successive cycles rather than with completely separated 11-year activity intervals. However, the calendar-time correspondence and the statistical timing alone do not establish that the high-latitude filaments belong magnetically to the following cycle.

4.3. Relation to previous filament and prominence studies

The broad latitude evolution found here is consistent with earlier studies showing that filaments and prominences contain several migration branches rather than a single sunspot-like butterfly pattern. In particular, Li et al. (2008) distinguished a poleward high-latitude branch, an equatorward migration from the polar region back toward intermediate latitudes after the polar phase, and the usual equatorward migration at low latitudes. Their interpretation places these branches in a broader full-disk activity cycle extending over more than one conventional sunspot cycle.

Prominence observations also show that the post-polar evolution can differ substantially between hemispheres and cycles. Shimojo et al. (2006) found that, after the polar-field reversal during Cycle 23, high-latitude prominence activity in the northern hemisphere migrated equatorward, whereas high-latitude activity persisted longer in the southern hemisphere. The latter behaviour became particularly unusual during the declining phase of Cycle 23: Shimojo (2013) reported prominence activity above 50°, and occasionally above 60°, even near the 2008 cycle minimum, and related this behaviour to the anomalous high-latitude magnetic-field distribution and weak polar field.

These results provide an important context for the late-cycle high-latitude population identified here. Our phase-normalized filament-area distribution does not show that the late-cycle increase in mean latitude is caused by a reversal of the equatorward migration of the main low-latitude population. Instead, the increase results from the changing relative contribution of filament area at high latitudes while the low-latitude population remains present. This does not contradict the equatorward post-polar migration reported in earlier studies, because our analysis does not track individual high-latitude structures or migration branches. It measures the statistical area distribution of all filaments present at a given phase.

Long-term prominence observations provide complementary evidence for the recurrent nature of the poleward branch. Using Kodaikanal, Meudon, and Kanzelhöhe observations over Solar Cycles 15–24, Chatterjee et al. (2020) identified poleward prominence migration in all ten cycles and found that the migration generally accelerates as the structures approach latitudes around 70°. Our analysis differs in that it uses the on-disk filament-area composite and concentrates on the relative contributions of latitude populations rather than on the polemost prominence trajectory.

The distinction is relevant when interpreting the late-cycle high-latitude signal. The operational threshold used here does not identify individual polar-crown filaments. The high-latitude population may therefore contain structures associated with different polarity-inversion-line systems. Nevertheless, its recurrent late-cycle enhancement and its systematic appearance before the following sunspot butterfly wing indicate that it forms a persistent part of the transition between successive activity cycles.

4.4. Implications and limitations

The systematic lead of high-latitude filament activity relative to the following sunspot wing raises the possibility that filaments may provide useful information on the early development of a new activity cycle. This should not yet be interpreted as a predictive relation. The butterfly-wing assignments used in the comparison are determined from the completed time–latitude distribution, and the present analysis is retrospective. In addition, the filament onset is defined statistically from an area distribution rather than from the first appearance of a particular magnetic structure.

The approximately 1–2 yr separations found here should consequently be regarded as characteristic temporal offsets between statistical activity patterns, rather than as forecast lead times. Establishing predictive value would require an onset criterion that can be applied without knowledge of the subsequent evolution and tested prospectively on independent cycles.

The relatively small number of independent cycles is another limitation. Although the filament composite covers ten cycles, the comparison with a following sunspot wing provides nine independent cycle transitions, SC15–SC23. The consistency of the temporal ordering, the exact randomization tests, the bootstrap confidence intervals, and the leave-one-cycle-out results all indicate that the effect is robust within this sample, but a larger number of independent cycles would be desirable.

A further limitation is the absence of magnetic information from the filament-area composite. Latitude and timing alone cannot establish whether the late-cycle high-latitude filaments are magnetically associated with the old cycle, the following cycle, or with large-scale polarity-inversion-line systems whose evolution does not map uniquely onto the conventional sunspot-cycle definition. Combining long-term filament observations with magnetic-polarity information would therefore provide an important next step. Such an analysis could test directly whether the high-latitude population identified here has a systematic magnetic relationship with the following activity cycle.

Despite these limitations, the recurrence of the late-cycle high-latitude population over many cycles and its systematic timing relative to the following sunspot butterfly wing indicate that the feature is not simply an artefact of cycle averaging. It appears to be a persistent component of the latitude–time evolution of solar filament activity and provides an additional observational perspective on the overlap between successive solar cycles.

5. Conclusions

We have analysed the latitude–time evolution of solar filament area over Solar Cycles 15–24 using the 1909–2022 composite Hα filament record of Chatzistergos et al. (2023b). By transforming individual cycles to a common normalized phase, we separated recurrent features of filament migration from differences in cycle duration and examined their stability over ten consecutive cycles.

The dominant low- and intermediate-latitude filament population shows the expected overall equatorward migration. The increase in mean absolute filament latitude observed during the declining part of the cycle does not represent a reversal of this migration. Instead, it is produced by the increasing contribution of a high-latitude filament population while low-latitude filament activity remains present. The late-cycle latitude increase therefore reflects the overlap of distinct components of the filament distribution.

Comparison with the independently identified sunspot butterfly wings of Leussu et al. (2017b) shows a systematic temporal relation between this high-latitude filament population and the following sunspot cycle. The high-latitude filament onset precedes the first identified sunspot groups of the following wing by approximately 1.1 yr on average and precedes the establishment of persistent following-cycle sunspot activity by approximately 2.2 yr. The latter ordering is found in all nine cycle transitions considered and is robust against reasonable changes in the definition of persistent sunspot-wing onset.

These results do not establish that the late-cycle high-latitude filaments belong magnetically to the following solar cycle. They do, however, demonstrate that their appearance systematically precedes the development of the following sunspot butterfly wing. High-latitude filament activity may therefore provide a useful tracer of the large-scale magnetic evolution occurring during the overlap and transition between successive solar activity cycles.

Acknowledgements

The author thanks T. Chatzistergos for helpful comments and clarifications regarding the composite filament data set.

Data Availability

The composite Hα filament-area data set used in this study is publicly available through the CDS/VizieR catalogue J/A+A/680/A15 (Chatzistergos et al. 2023a), https://doi.org/10.26093/cds/vizier.36800015.

The separated sunspot butterfly-wing data are publicly available through the CDS/VizieR catalogue J/A+A/599/A131 (Leussu et al. 2017a), https://doi.org/10.26093/cds/vizier.35990131.

Funding

The author received no specific funding for this work.

Competing Interests

The author declares no competing interests.

References

Bocchino, G. (1933). Migrazione delle protuberanze durante il ciclo undecennale dell'attività solare. *Osservazioni e Memorie dell'Osservatorio Astrofisico di Arcetri*, 51:5–47.

Chatterjee, S., Hegde, M., Banerjee, D., Ravindra, B., and McIntosh, S. W. (2020). Time-latitude distribution of prominences for 10 solar cycles: A study using kodaikanal, meudon, and kanzelhohe data. *Earth and Space Science*, 7(3):e2019EA000666.

Chatzistergos, T., Ermolli, I., Banerjee, D., Barata, T., Chouinavas, I., Falco, M., Gafeira, R., Giorgi, F., Hanaoka, Y., Krivova, N. A., Korokhin, V. V., Lourenço, A., Marchenko, G. P., Malherbe, J.-M., Peixinho, N., Romano, P., and Sakurai, T. (2023a). 1909–2022 carrington filament properties [data set]. CDS/VizieR catalogue J/A+A/680/A15.

Chatzistergos, T., Ermolli, I., Banerjee, D., Barata, T., Chouinavas, I., Falco, M., Gafeira, R., Giorgi, F., Hanaoka, Y., Krivova, N. A., Korokhin, V. V., Lourenço, A., Marchenko, G. P., Malherbe, J.-M., Peixinho, N., Romano, P., and Sakurai, T. (2023b). Analysis of full-disc hα observations: Carrington maps and filament properties in 1909–2022. *Astronomy & Astrophysics*, 680:A15.

Gibson, S. E. (2018). Solar prominences: theory and models. *Living Reviews in Solar Physics*, 15:7.

Hanaoka, Y. and Sakurai, T. (2017). Statistical study of the magnetic field orientation in solar filaments. *The Astrophysical Journal*, 851(2):130.

Hyder, C. L. (1965). The polar crown of filaments and the sun's polar magnetic fields. *The Astrophysical Journal*, 141:272.

Labrosse, N., Heinzel, P., Vial, J.-C., Kucera, T., Parenti, S., Gunár, S., Schmieder, B., and Kilper, G. (2010). Physics of solar prominences: I—spectral diagnostics and non-lte modelling. *Space Science Reviews*, 151(4):243–332.

Leussu, R., Usoskin, I. G., Arlt, R., and Mursula, K. (2016). Properties of sunspot cycles and hemispheric wings since the 19th century. *Astronomy & Astrophysics*, 592:A160.

Leussu, R., Usoskin, I. G., Senthamizh Pavai, V., Diercke, A., Arlt, R., and Mursula, K. (2017a). Butterfly diagram wings [data set]. CDS/VizieR catalogue J/A+A/599/A131.

Leussu, R., Usoskin, I. G., Senthamizh Pavai, V., Diercke, A., Arlt, R., and Mursula, K. (2017b). Wings of the butterfly: Sunspot groups for 1826–2015. *Astronomy & Astrophysics*, 599:A131.

Li, K. J. (2010). Latitude migration of solar filaments. *Monthly Notices of the Royal Astronomical Society*, 405(2):1040–1046.

Li, K. J., Li, Q. X., Gao, P. X., and Shi, X. J. (2008). Cyclic behavior of solar full-disk activity. *Journal of Geophysical Research: Space Physics*, 113:A11108.

Mackay, D. H., Karpen, J. T., Ballester, J. L., Schmieder, B., and Aulanier, G. (2010). Physics of solar prominences: Ii—magnetic structure and dynamics. *Space Science Reviews*, 151(4):333–399.

Mazumder, R., Bhowmik, P., and Nandy, D. (2018). The association of filaments, polarity inversion lines, and coronal hole properties with the sunspot cycle: An analysis of the mcintosh database. *The Astrophysical Journal*, 868(1):52.

McIntosh, S. W., Leamon, R. J., Egeland, R., Dikpati, M., Altrock, R. C., Banerjee, D., Chatterjee, S., Srivastava, A. K., and Velli, M. (2021). Deciphering solar magnetic activity: 140 years of the 'extended solar cycle'—mapping the hale cycle. *Solar Physics*, 296:189.

Meunier, N. and Delfosse, X. (2011). Filaments and the magnetic configuration. i. observation of the solar case. *Astronomy & Astrophysics*, 532:A18.

Minarovjech, M., Rybanský, M., and Rušin, V. (1998). Time-latitude prominence and the green corona distribution over the solar activity cycle. In *New Perspectives on Solar Prominences*, volume 150 of *Astronomical Society of the Pacific Conference Series*, pages 484–487.

Mouradian, Z. and Soru-Escaut, I. (1994). A new analysis of the butterfly diagram for solar filaments. *Astronomy & Astrophysics*, 290:279.

Petrie, G. J. D. (2015). Solar magnetism in the polar regions. *Living Reviews in Solar Physics*, 12:5.

Routh, S., Pal, S., Nandy, D., Chatterjee, S., Banerjee, D., and Khan, M. S. (2025). Polar filaments capture high-latitude solar poloidal field interactions and can foretell the future sunspot cycle amplitude before polar field precursors. *The Astrophysical Journal Letters*, 993(2):L44.

Shimojo, M. (2013). Unusual migration of prominence activities in the southern hemisphere during cycles 23–24. *Publications of the Astronomical Society of Japan*, 65(sp1):S16.

Shimojo, M., Yokoyama, T., Asai, A., Nakajima, H., and Shibasaki, K. (2006). One solar-cycle observations of prominence activities using the nobeyama radioheliograph 1992–2004. *Publications of the Astronomical Society of Japan*, 58(1):85–92.

Takalo, J. (2021a). Comparison of geomagnetic indices during even and odd solar cycles sc17–sc24: Signatures of gnevyshev gap in geomagnetic activity. *Solar Physics*, 296:19.

Takalo, J. J. (2021b). Temporal distribution of solar cycle 24 sunspot groups: Comparison to cycles 12–23. *Annals of Geophysics*, 64(1):DM107.

Tandberg-Hanssen, E. (1995). *The Nature of Solar Prominences*. Kluwer Academic Publishers.